

8. Ramasastry, C. & Ramaiah, A. S. Electrical conduction in  $\text{Na}_3\text{H}(\text{SO}_4)_2$  crystals. *J. Mater. Sci. Lett.* **16**, 2011–2016 (1981).
9. Chisholm, C. R. I., Merinov, B. V. & Haile, S. M. High temperature phase transitions in  $\text{K}_3\text{H}(\text{SO}_4)_2$ . *Solid State Ion.* (in the press).
10. Gaskell, D. R. *Introduction to Metallurgical Thermodynamics* 2nd edn, 574 & 586 (McGraw-Hill, Washington DC, 1981).
11. Srinivasan, S., Velev, O. A., Parthasarathy, A., Manko, D. J. & Appleby, A. J. High energy efficiency and high power density proton exchange membrane fuel cells—electrode kinetics and mass transport. *J. Power Sources* **36**, 299–320 (1991).
12. Croce, F. & Cigna, G. Determination of the protonic transference number for  $\text{KH}_2\text{PO}_4$  by electromotive force measurements. *Solid State Ion.* **6**, 201–202 (1982).
13. Minh, N. Q. Ceramic fuel cells. *J. Am. Ceram. Soc.* **76**, 563–588 (1993).
14. Minh, N. Q. & Horne, C. R. in *Proc. 14th Riso Int. Symp. on Materials Science: High Temperature Electrochemical Behaviour of Fast Ion and Mixed Conductors* (eds Poulsen, F. W., Bentzen, J. J., Jacobsen, T., Skou, E. & Østergård, M. J. L.) 337–341 (Riso National Laboratory, Roskilde, 1993).
15. Baranov, A. I., Khiznichenko, V. P., Sandler, V. A. & Shuvalov, L. A. Frequency dielectric dispersion in the ferroelectric and superionic phases of  $\text{CsH}_2\text{PO}_4$ . *Ferroelectrics* **81**, 183–186 (1988).
16. Slade, R. C. T. & Omana, M. J. Protonic conductivity of 12-tungstophosphoric acid (TPA,  $\text{H}_3\text{PW}_{12}\text{O}_{40}$ ) at elevated temperatures. *Solid State Ion.* **58**, 195–199 (1992).
17. Haile, S. M., Narayanan, S. R., Chisholm, C. & Boysen, D. Proton conducting membrane using a solid acid. US patent 09/439,377 (15 Nov. 2000).

Supplementary information is available on Nature's World-Wide Web site (<http://www.nature.com>) or as paper copy from the London editorial office of Nature.

### Acknowledgements

We thank J. Snyder for assistance with computer automation of the fuel cell test station and S. R. Narayanan for technical discussions. Financial support has been provided by the California Institute of Technology through the Yuen Grubstake entrepreneurial fund.

Correspondence and requests for materials should be addressed to S.M.H. (e-mail: [smhaile@caltech.edu](mailto:smhaile@caltech.edu)).

## Self-assembly of mesoscopically ordered chromatic polydiacetylene/silica nanocomposites

Yunfeng Lu<sup>\*†‡§</sup>, Yi Yang<sup>†</sup>, Alan Sellinger<sup>‡§</sup>, Mengcheng Lu<sup>†</sup>, Jinman Huang<sup>†</sup>, Hongyou Fan<sup>‡</sup>, Raid Haddad<sup>†</sup>, Gabriel Lopez<sup>†</sup>, Alan R. Burns<sup>‡</sup>, Darryl Y. Sasaki<sup>‡</sup>, John Shelnutt<sup>‡</sup> & C. Jeffrey Brinker<sup>†‡§</sup>

<sup>†</sup>The University of New Mexico Center for Micro-Engineered Materials and Department of Chemical and Nuclear Engineering, Albuquerque, New Mexico 87131, USA

<sup>‡</sup>Sandia National Laboratories, Advanced Materials Laboratory, 1001 University Blvd SE, Albuquerque, New Mexico 87106, USA

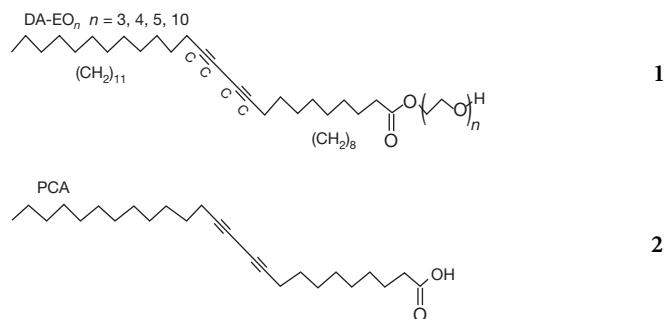
<sup>§</sup>These authors contributed equally to this work.

Nature abounds with intricate composite architectures composed of hard and soft materials synergistically intertwined to provide both useful functionality and mechanical integrity. Recent synthetic efforts to mimic such natural designs have focused on nanocomposites<sup>1–5</sup>, prepared mainly by slow procedures like monomer or polymer infiltration of inorganic nanostructures<sup>6,7</sup> or sequential deposition<sup>8,9</sup>. Here we report the self-assembly of conjugated polymer/silica nanocomposite films with hexagonal, cubic or lamellar mesoscopic order using polymerizable amphiphilic diacetylene molecules as both structure-directing agents and monomers. The self-assembly procedure is rapid and incorporates the organic monomers uniformly within a highly

ordered, inorganic environment. Polymerization results in polydiacetylene/silica nanocomposites that are optically transparent and mechanically robust. Compared to ordered diacetylene-containing films prepared as Langmuir monolayers<sup>10</sup> or by Langmuir–Blodgett deposition<sup>10</sup>, the nanostructured inorganic host alters the diacetylene polymerization behaviour, and the resulting nanocomposite exhibits unusual chromatic changes in response to thermal, mechanical and chemical stimuli. The inorganic framework serves to protect, stabilize, and orient the polymer, and to mediate its function. The nanocomposite architecture also provides sufficient mechanical integrity to enable integration into devices and microsystems.

Owing to extended  $\pi$ -electron delocalization along their backbones, conjugated organic polymers exhibit electronic and optical properties of interest for applications ranging from light-emitting diodes to biomolecular sensors<sup>11</sup>. For example, in blue-coloured polydiacetylene, the optical absorption blue-shifts dramatically when stress is applied to the backbone through the pendant side chains, and this thermally, mechanically, or chemically induced chromatic (blue  $\rightarrow$  red) response has been explored as a colorimetric transduction scheme in a variety of chemically and physically based sensor designs<sup>12,13</sup>. Further improvements of the electronic and optical performance of conjugated polymer devices may require polymer incorporation in nano-engineered architectures<sup>14</sup> that could provide alignment, control charge and energy transfer, mediate conformational changes and prevent oxidation. Recently control of energy transfer was demonstrated in a poly[2-methoxy-5-(2'-ethyl-hexyloxy)-1,4-phenylene vinylene] (MEH-PPV)/silica nanocomposite<sup>7</sup>. However, this nanocomposite, prepared by MEH-PPV infiltration of a pre-formed, oriented, hexagonal, silica mesophase, was heterogeneous, exhibiting two distinct conjugated polymer environments, that is, polymers inside and outside the hexagonally arranged pore channels of the silica particles. In general, because polymer infiltration into a pre-formed porous nanostructure depends on the partitioning of the polymer from the solvent, we expect it to be difficult to control polymer concentration, orientation and uniformity in the corresponding nanocomposite. Further, when the nanostructure pore size is less than the radius of gyration of the solvated polymer, infiltration proceeds by a worm-like motion referred to as reptation, requiring long processing times at elevated temperatures<sup>7</sup>.

We use a series of oligoethylene glycol functionalized diacetylenic (DA-EO<sub>n</sub>) surfactants (structure 1, with  $n = 3, 4, 5, 10$ ), prepared by coupling ethylene glycols with the acid chloride of PCA (structure 2)



both as amphiphiles to direct the self-assembly of thin film silica mesophases<sup>15</sup> and as monomeric precursors of the conjugated polymer, polydiacetylene (PDA). Beginning with a homogeneous solution of silicic acid and surfactant prepared in a tetrahydrofuran (THF)/water solvent with initial surfactant concentration  $c_0$  much less than the critical surfactant micelle concentration CMC, we use evaporative dip-coating, spin-coating, or casting procedures to prepare thin films on silicon (100) or fused silica substrates (Fig. 1). During deposition, preferential evaporation of THF

<sup>§</sup> Present address: Tulane University Chemical Engineering Department, New Orleans, Louisiana 70118, USA (Y.L.); Canon Research and Development Center Americas, San Jose, California 95134, USA (A.S.).

concentrates the depositing film in water and nonvolatile silica and surfactant species. The progressively increasing surfactant concentration drives self-assembly of diacetylene/silica surfactant micelles and their further organization into ordered, three-dimensional, liquid crystalline mesophases. Ultraviolet-light-initiated polymerization of the DA units, accompanied by catalyst-promoted siloxane condensation, topochemically converts the colourless mesophase into the blue PDA/silica nanocomposite, preserving the highly ordered, self-assembled architecture.

The choice of surfactant greatly influences the resultant mesostructure. This is evident from the X-ray diffraction (XRD) patterns and TEM micrographs shown in Figs 2 and 3 for nanocomposites prepared from diacetylenic surfactants with tri ( $n = 3$ ), penta ( $n = 5$ ) and decaethylene ( $n = 10$ ) glycol head groups. Increasing values of  $n$  increase the surfactant head group area  $a_0$ . This in turn reduces the value of the surfactant packing parameter,  $g = v/a_0l$ , where  $v$  is the surfactant volume and  $l$  the tail length<sup>16</sup>, favouring the formation of progressively higher-curvature mesophases: lamellar ( $n = 3$ )  $\rightarrow$  hexagonal ( $n = 5$ )  $\rightarrow$  cubic ( $n = 10$ ). From the highly ordered nanocomposite mesostructures observed by transmission electron microscopy (TEM), we infer that the surfactant monomers/structure-directing agents are uniformly

organized into precise spatial arrangements before polymerization. These arrangements establish the proximity (topochemistry) of the reactive diacetylenic moieties and thus strongly influence the PDA polymerization process. This is best illustrated by comparing their polymerization behaviour, as shown by the blue (or red) colour of nanocomposite films prepared with different mesostructures (that is, the hexagonal, cubic, and lamellar mesostructures shown in Fig. 3) and contrasting these behaviours with those of planar self-assembled monolayer and trilayer films formed by Langmuir–Blodgett deposition of the neat DA surfactants.

Figure 4 shows a patterned blue PDA/silica nanocomposite film, with a hexagonal mesostructure (prepared using structure 1, with  $n = 5$ ), formed by ultraviolet exposure through a mask; the corresponding patterned red film was formed subsequently by heating to 100 °C (Fig. 4b). Whereas lamellar mesophases (prepared using structure 1 with  $n = 3$ ) show qualitatively similar behaviour, cubic mesostructures (prepared using structure 1 with  $n = 10$ ) and Langmuir monolayers and trilayers (prepared using neat 1 with  $n = 3, 5$  or 10) remain colourless upon ultraviolet exposure and during heating. The different behaviour of lamellar and Langmuir films emphasize the importance of the nanostructured inorganic host on PDA polymerization. In both systems the diacetylenic

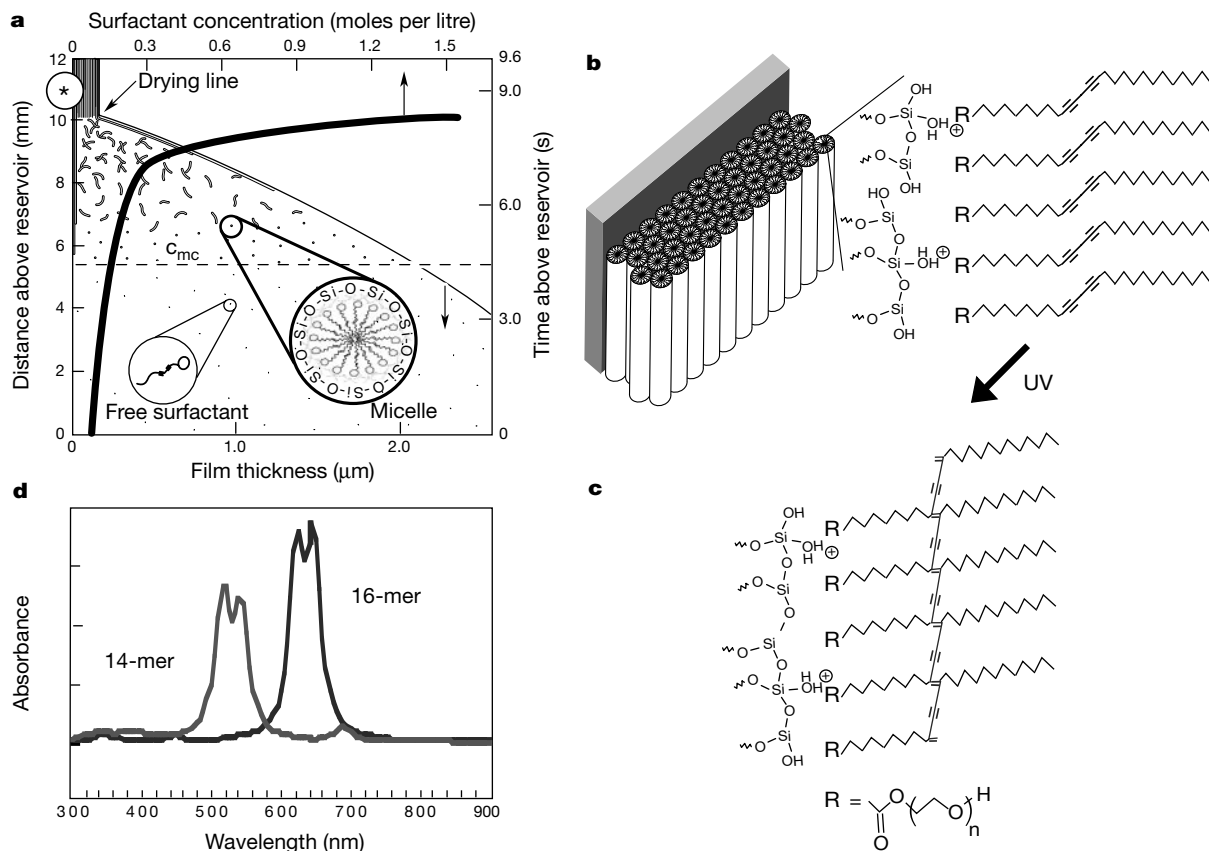


**Figure 1** Schematic representation of the PDA/silica nanocomposite evaporation-induced self-assembly process. **a**, Steady-state film thickness and surfactant concentration profiles developed during dip-coating, with vertical axes representing distance and time above reservoir surface and horizontal axes showing film thickness and surfactant (structures 1 or 2) concentration for  $c_0 = 0.034$  M. Beginning with a homogeneous solution prepared with  $c_0 < CMC$ , preferential THF evaporation induces micellization and further self-organization of silica–surfactant composite micelles into ordered thin-film mesophases. The shape and concentration of the DA surfactants influence the mesophase established at the drying line (lamellar, hexagonal or cubic). **b**, Section near asterisk shows a hexagonal mesostructure and hypothetical arrangement of DA

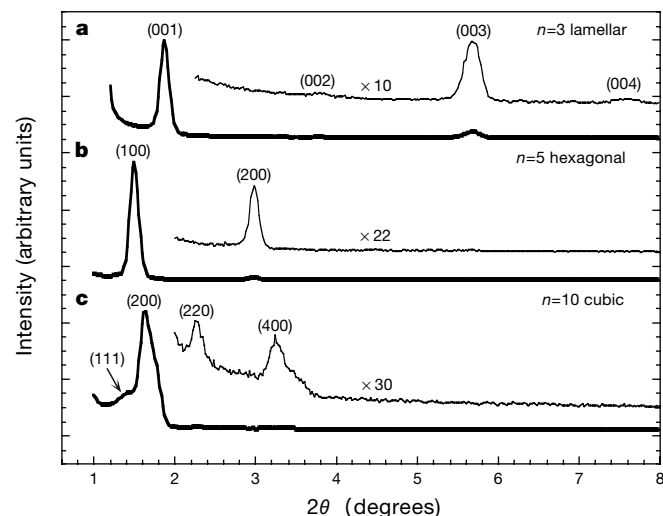
surfactants adjacent to the cylindrically structured silicic acid framework. **c**, Hypothetical structure of polymerized PDA/silica nanocomposite formed upon exposure to ultraviolet light and continued acid-catalysed siloxane condensation. **d**, Ultraviolet–visible spectra of cyclic polydiacetylene oligomers determined by INDO/S (Intermediate Neglect Differential Orbital Spectra) quantum calculations after energy-optimization and 10 ps of molecular dynamics. The 16-membered oligomer with diameter of about 2.4 nm absorbs in the red region of the visual spectrum with spectral characteristics commensurate with the blue form of PDA (compare with Fig. 4e). The higher-curvature 14-membered PDA oligomer is strained and has a blue-shifted absorption spectrum consistent with the red form of PDA (compare with Fig. 4e).

surfactants are organized into highly oriented planar configurations with the EO headgroups disposed toward the hydrophilic interface, either water (Langmuir films) or polysilicic acid (nanocomposites). Despite these similar organizations, we suggest that Langmuir films do not polymerize because the reactive DA moieties are spaced too far apart, as indicated by the molecular areas measured at 30 mN m<sup>-1</sup> in a Langmuir trough: DA-EO<sub>1</sub> = 24 Å<sup>2</sup>, DA-EO<sub>3</sub> = 38 Å<sup>2</sup>, DA-EO<sub>5</sub> = 46 Å<sup>2</sup>. Closer spacing of the EO headgroups (and correspondingly the diacetylenic moieties) within the self-assembled nanocomposites (lamellar, hexagonal or cubic) is anticipated from the requirement for charge density matching at the R-EO<sub>*n*-*y*</sub>[EO·H<sub>3</sub>O<sup>+</sup>]<sub>*y*</sub>·*y*X<sup>-</sup>·*w*I<sup>δ+</sup> interface (where R = alkyl chain, *y* ≤ *n*, X = Cl<sup>-</sup>, I<sup>δ+</sup> = the silica framework carrying a partial charge of δ<sup>+</sup>, and *w* is the ‘concentration’ of framework needed for charge balance) that reduces the optimal EO headgroup area *a*<sub>0</sub> (ref. 17). This closer spacing is reflected in measurements of the biaxial stress resulting from PDA polymerization, where, for nanocomposites, we observe development of compressive stress upon polymerization (film turns blue) and during the solvatochromic or thermochromic blue → red transformation; this indicates a net expansion of the PDA relative to the silica host (see Fig. A in the Supplementary Information). The corresponding neat DA surfactants prepared as Langmuir monolayers do not polymerize and develop no stress upon ultraviolet irradiation. Polymerizable DA Langmuir monolayers and multilayers (prepared using surfactants with smaller headgroups) contract upon polymerization and the magnitude of this

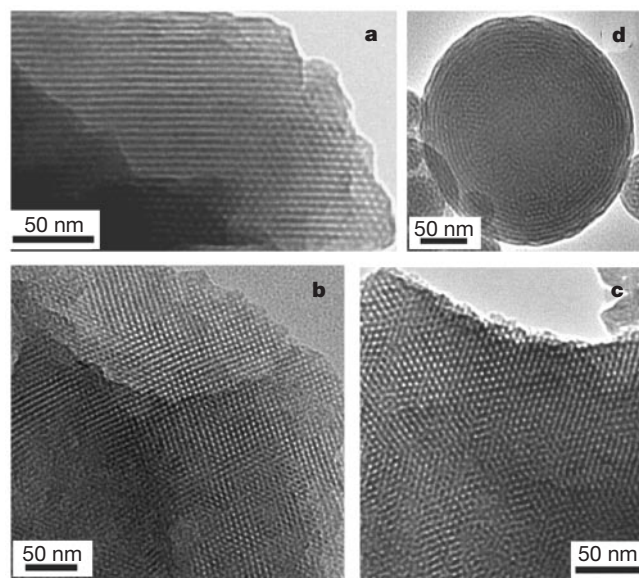
contraction is used to assess the extent of polymerization<sup>18</sup>.

The importance of the proximity of the DA moieties on polymerization is further illustrated by our inability to polymerize DA within the cubic mesophase prepared with *n* = 10 (see Fig. 3b and c). The large EO<sub>10</sub> surfactant headgroups are necessary to direct the formation of the cubic mesophase, but they also serve as spacers preventing polymerization. Introduction of structure 1, with *n* = 3 or 5 or structure 2 as co-surfactants with smaller headgroups (30–50 wt% relative to EO-DA<sub>10</sub>) allows us to form cubic mesophases and to polymerize the mixed surfactant assemblies into the blue and red forms of PDA. (We expect that, owing to phase separation<sup>19</sup>, this is not possible in Langmuir monolayers or Langmuir–Blodgett films).

The polymerization of the surfactant is highly dependent upon the topological alignment of diacetylenic units within the supramolecular assembly<sup>20,21</sup>. Additionally, for colorimetric materials to form (especially blue-coloured materials), the degree of polymerization and conjugation length of the ‘ene’–‘yne’ backbone must be considerable<sup>22</sup>. The micellar structures that template the silica sol-gel material must thus contain highly oriented, densely packed surfactants. This packing will allow facile topochemical polymerization of the diacetylene units to give coloured polydiacetylene.



**Figure 2** X-ray diffraction (XRD) patterns of nanocomposite thin films prepared using DA-EO<sub>*n*</sub> (where *n* = 3, 5, and 10) surfactants. Increasing values of *n* increase the surfactant head group favouring the formation of progressively higher-curvature mesophases: lamellar (*n* = 3) → hexagonal (*n* = 5) → cubic (*n* = 10). **a**, Film prepared using 1.86% of DA-EO<sub>3</sub> (wt% DA-EO<sub>3</sub> relative to the solution weight without surfactant) shows a lamellar mesostructure with (001) diffraction peak at 48 Å. The presence of higher-order diffraction peaks (002), (003) and (004) indicate the formation of highly ordered alternating silica/PDA layers. **b**, Film prepared with DA-EO<sub>5</sub> (2.23%) shows a hexagonal mesophase with strong (100) and (200) diffraction peaks at 56 Å and 28 Å, respectively. **c**, Film prepared using 2.23% DA-EO<sub>10</sub> surfactant exhibits a cubic mesophase with unit-cell parameter *a* = 108.1 Å. The presence of the (111) diffraction peak at 62.4 Å and the (200) diffraction peak at 54.1 Å clearly establishes a face-centred or primary cubic structure. The presence of higher-order peaks (220) at 38.2 Å and (400) at 27.3 Å provide further evidence of the primary or face-centred cubic mesophase. Introduction of structure 1, with *n* = 3 or 5 or structure 2, as co-surfactants with smaller headgroups (30–50 wt% relative to EO-DA<sub>10</sub>) was necessary to polymerize PDA in the blue or red forms within the cubic mesophase. The XRD patterns were essentially unchanged by these co-surfactant additions.



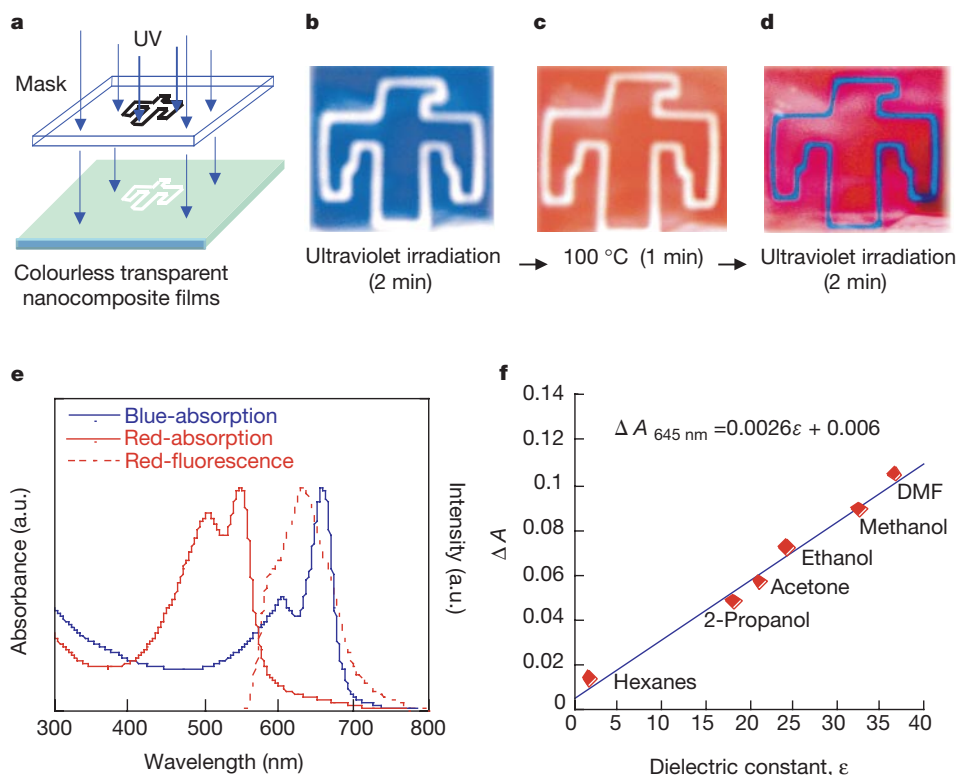
**Figure 3** Representative transmission electron microscope (TEM) images of nanocomposite thin films (prepared as in Fig. 2b and c) and particles (formed by a related aerosol-assisted evaporation-induced self-assembly approach<sup>32</sup>). **a**, Hexagonally ordered nanocomposite prepared using 2.23% DA-EO<sub>5</sub> surfactant, showing a striped [110]-oriented mesophase with repeat distance around 48 Å and a region of the corresponding hexagonally patterned mesostructure characteristic of the [001]-orientation (right edge). The smaller spacing measured by TEM versus XRD (48 Å versus 56 Å, compare **a** and Fig. 2b) may be due to the over-focus condition used to achieve high contrast in TEM or electron-beam-induced shrinkage (normal to the substrate) which can occur in general for uncalcined, mesostructured materials. **b, c**, Two orientations of a cubic nanocomposite film prepared using 2.23% DA-EO<sub>10</sub> surfactant. A highly ordered [100] orientation with unit-cell parameter at 108 Å, agreeing well with the XRD results. **c**, The corresponding [111] orientation with repeat distance of 62 Å. As for the corresponding XRD patterns, the cubic mesostructures revealed by TEM were quite comparable with and without the addition of co-surfactants (structure 1, with *n* = 3 or 5, or structure 2) needed to polymerize the blue or red forms of PDA within the cubic mesostructure. **d**, PDA/silica nanocomposite particles prepared using an aerosol-assisted evaporation-induced self-assembly technique<sup>32</sup>. The particle exhibits an ordered multi-lamellar exterior and a disordered worm-like mesostructured interior, consistent with a radially directed self-assembly process.

Figure 1 illustrates a postulated length-wise polymerization of surfactants within a cylindrical rod-like micelle to yield the blue form of PDA. Circumferential polymerization, although favoured on the basis of proximity of reactive DA moieties, would impose a high curvature on the PDA backbone because of the small pore size of the mesostructured host (2.5–3.0 nm in diameter, see Fig. B in the Supplementary Information). Although DA surfactants organized into ellipsoidal liposomes (40 nm × 15 nm) are known to polymerize in the blue and red forms<sup>23</sup> we questioned whether circumferential arrangements of DA surfactants (within spherical or cylindrical micelles) could polymerize with the proper ‘ene’–‘yne’ conjugation to produce coloured materials. Molecular mechanics and dynamics calculations indicate that cyclic arrangements of up to 19 DA monomers around the periphery of the 3.0-nm-diameter pore are possible and that an energy-optimized 16-membered cyclic PDA oligomer can exhibit absorption behaviour consistent with the blue form of PDA (see Fig. 1d). Helical conformations<sup>24</sup> represent an alternative configuration that might satisfy DA proximity requirements without severely disrupting the conjugation. In general, nonlinear conformations may be needed for polymer propagation within these self-assembled nano-structured hosts. Such conformations are presumably rare or impossible for Langmuir monolayers and Langmuir–Blodgett films.

The PDA/silica nanocomposite films are optically transparent and mechanically robust. Modulus values measured by nano-indentation ( $3.50 \pm 1.00$  GPa) are compared to those of calcined mesoporous silica films that have been successfully integrated into microelectronic devices as low dielectric constant films (Y.L. and

C.J.B., unpublished work). Nitrogen sorption experiments performed using a surface acoustic wave technique<sup>25</sup> show the nanocomposite films to be nonporous to nitrogen at  $-196$  °C (Type II sorption isotherm, see Fig. B of the Supplementary Information), meaning that the PDA completely fills the pore channels and that the composite architecture may impart some degree of oxidation resistance (important for extension to other conjugated polymer nanocomposites).

The blue PDA/silica nanocomposites thus exhibit solvatochromic, thermochromic, and mechanochromic properties. When contacted with the series of polar solvents—2-propanol, acetone, ethanol, methanol and dimethylformamide—the films transform to the red, fluorescent form and the differential absorbance ( $A$ ) at 645 nm ( $A_{\text{blue}} - A_{\text{red}}$ ) scales linearly with the dielectric constant of the solvent:  $A_{645\text{ nm}} = 0.003$  (dielectric constant)  $- 0.005$ ; for a correlation coefficient of 0.992 (see Fig. 4f), suggesting applications in sensing. We suggest that polar solvents diffuse within the polar, hydrophilic  $\text{EO}_n$  pendant side chains. The accompanying solvation stresses are transferred to the PDA backbone (evidence for solvation stresses are presented in Fig. A of the Supplementary Information), reducing its conjugation length, and therefore inducing the blue  $\rightarrow$  red transformation<sup>26</sup> as understood by recent molecular mechanics simulations<sup>27</sup>. The solvatochromic behaviour shows very slow reversibility. Heating to temperatures in excess of 47 °C can also cause the blue  $\rightarrow$  red transformation, and preliminary results have shown this thermochromic behaviour to be rapidly reversible (several seconds). This may arise from hydrogen-bonding interactions<sup>26</sup> of the pendant side chains with the silanol moieties



**Figure 4** Patterned polymerization induced by ultraviolet irradiation and the thermochromic and solvatochromic transition of a hexagonal PDA/silica nanocomposite film. **a**, Schematic representation of the ultraviolet patterning procedure. **b**, Patterned blue/colourless film formed by ultraviolet irradiation for 2 min. **c**, Patterned red/colourless film formed by heating the film in **b** to 100 °C for 1 min. **d**, Patterned red/blue film formed by ultraviolet exposure of film in **c** for 2 min. **e**, Ultraviolet–visible spectra of the blue PDA/silica hexagonally ordered nanocomposite, the corresponding red film formed by heating at 100 °C, and the fluorescence emission spectrum of the red film (excited at 500 nm).

Film formed from structure **1**, with  $n = 5$ . **f**, Differential absorbance at 645 nm resulting from the solvatochromic transition of blue PDA/silica nanocomposite films to the corresponding red films upon immersion of the blue films in the series of solvents: hexane, 2-propanol, acetone, ethanol, methanol, or dimethylformamide. Immersion times were 3 s followed by drying in nitrogen at room temperature. Without consideration of the non-polar solvent, hexane, the regression equation is  $A_{645\text{ nm}} = 0.003$  (dielectric constant)  $- 0.005$ , correlation coefficient = 0.992.

of the surrounding inorganic mesophase, supplying a restoring force and enabling recovery of the original side-chain orientation. Mechanical abrasion of the blue nanocomposite film causes local transformation to the red fluorescent form. Thus we envision mechanochromic barrier coatings that could sense excessive mechanical damage by changing from the blue form to the red fluorescent form.

The use of polymerizable surfactants as both structure-directing agents and monomers in the various evaporation-driven self-assembly schemes developed recently<sup>28,29</sup> represents a general, efficient route to the formation of robust and functional nanocomposites. Synthesis of surfactants with polymerizable thiophene, acetylene or phenylenevinylene groups should enable the self-assembly of conductive, conjugated polymer/silica nanocomposites in thin-film forms suitable for integration into devices. Conductive polymers confined within rod-like micellar channels of an electrical insulator conjure ideas of molecular wires. Unlike conduction measurements with two-dimensional films, such as bilayers<sup>30</sup> and monolayers<sup>31</sup>, hexagonally ordered nanocomposite mesophases are nearly one-dimensional structures that could allow efficient conductivity along the channel direction. □

**Methods**

Precursor solutions were synthesized from tetraethylorthosilicate (TEOS, Si(OC<sub>2</sub>H<sub>5</sub>)<sub>4</sub>), diacetylenic surfactants (structure 1 with n = 3, 4, 5, 10; structure 2, or combinations thereof) and HCl catalyst prepared in a THF/water solvent. The final reactant mole ratios were 1 TEOS:31.4–57.9 THF:4.96 H<sub>2</sub>O:0.013 HCl:0.06–1.41 DA surfactant. Films were prepared by casting, spin-coating at 2,000 r.p.m., or dip-coating at a rate of 40 cm min<sup>-1</sup>. Polymerization of PDA to the blue form was done by ultraviolet exposure at 266 nm for times ranging from 30 s to 30 min. Subsequent transformation to the red form was accomplished by heating at 100 °C for times ranging from 30 s to 2 min or by exposure to a solvent.

Molecular simulations were performed using Cerius<sup>2</sup> and Polygraf software and the Burchart–Dreiding 2.21 force field. Ultraviolet–visible spectra of the PDA oligomers were calculated from the transition wavelengths and oscillator strengths obtained from INDO/S calculations on the terminated polymer backbone structure obtained from the molecular dynamics calculation.

Received 3 November 2000; accepted 6 February 2001.

1. Dagani, R. Putting the “nano” into composites. *Chem. Eng. News* **77**, 25–37 (1999).
2. Giannelis, E. Polymer layered silicate nanocomposites. *Adv. Mater.* **8**, 29–35 (1996).
3. Asefa, T., Yoshina-Ishii, C., MacLachlan, M. J. & Ozin, G. A. New nanocomposites: putting organic function “inside” the channel walls of periodic mesoporous silica. *J. Mater. Chem.* **10**, 1751–1755 (2000).
4. Smith, R. C., Fischer, W. M. & Glin, D. L. Ordered poly(*p*-phenylenevinylene) matrix nanocomposites via lyotropic liquid-crystalline monomers. *J. Am. Chem. Soc.* **119**, 4092–4093 (1997).
5. Sellinger, A. *et al.* Continuous self-assembly of organic-inorganic nanocomposite coatings that mimic nacre. *Nature* **394**, 256–260 (1998).
6. Moller, K., Bein, T. & Fischer, R. X. Entrapment of PMMA polymer strands in micro- and mesoporous materials. *Chem. Mater.* **10**, 1841–1852 (1998).
7. Nguyen, T.-Q., Wu, J., Doan, V., Schwartz, B. J. & Tolbert, S. H. Control of energy transfer in oriented conjugated polymer-mesoporous silica composites. *Science* **288**, 652–656 (2000).
8. Kleinfeld, E. R. & Ferguson, G. S. Stepwise formation of multilayered nanostructural films from macromolecular precursors. *Science* **265**, 370–373 (1994).
9. Keller, S. W., Kim, H.-N. & Mallouk, T. E. Layer-by-layer assembly of intercalation compounds and heterostructures on surfaces: Toward molecular “beaker” epitaxy. *J. Am. Chem. Soc.* **116**, 8817–8818 (1994).
10. Sasaki, D. Y., Carpick, R. W. & Burns, A. R. High molecular orientation in mono- and trilayer polydiacetylene films imaged by atomic force microscopy. *J. Colloid Interf. Sci.* **229**, 490–496 (2000).
11. Charych, D., Nagy, J., Spevak, W. & Bednarski, M. Direct colorimetric detection of a receptor-ligand interaction by a polymerized bilayer assembly. *Science* **261**, 585–588 (1993).
12. Cheng, Q. & Stevens, R. Charge-induced chromatic transition of amino acid-derivatized polydiacetylene liposomes. *Langmuir* **14**, 1974–1976 (1998).
13. Cheng, Q., Yamamoto, M. & Stevens, R. Amino acid terminated polydiacetylene lipid microstructures: morphology and chromatic transition. *Langmuir* **16**, 5333–5342 (2000).
14. Mazumdar, S. Prospects for the polymer nanoengineer. *Science* **288**, 630–631 (2000).
15. Lu, Y. F. *et al.* Continuous formation of supported cubic and hexagonal mesoporous films by sol-gel dip coating. *Nature* **389**, 364–368 (1997).
16. Israelachvili, J. N. *Intermolecular and Surface Forces* Ch. 17 (Academic, San Diego, 1992).
17. Monnier, A. *et al.* Cooperative formation of inorganic-organic interfaces in the synthesis of silicate mesostructures. *Science* **261**, 1299–1303 (1993).
18. Day, D. & Ringsdorf, H. Polymerization of diacetylene carbonic acid monolayers at the gas-water interface. *J. Polym. Sci. Polym. Lett. Edn* **16**, 205–210 (1978).
19. Gaines, G. L. (ed.) in *Insoluble Monolayers at Liquid-Gas Interfaces* 281–300 (John Wiley, New York, 1966).
20. Menzel, H., Mowery, M. D., Cai, M. & Evans, C. E. Vertical positioning of internal molecular scaffolding within a single molecular layer. *J. Phys. Chem. B* **102**, 9550–9556 (1998).

21. Collins, M. Optical-properties of poly-diacetylene monolayers. *J. Polym. Sci. B* **26**, 367–372 (1988).
22. Kuriyama, K., Kikuchi, H. & Kajiyama, T. Molecular packings-photopolymerization behavior relationship of diacetylene Langmuir-Blodgett films. *Langmuir* **12**, 6468–6472 (1996).
23. Spevak, W. *et al.* Polymerized liposomes containing C-glycosides of sialic acid: Potent inhibitors of influenza virus in vitro infectivity. *J. Am. Chem. Soc.* **115**, 1146–1147 (1993).
24. Frankel, D. A. & O’Brien, D. F. Supramolecular assemblies of diacetylenic aldonamides. *J. Am. Chem. Soc.* **113**, 7436–7437 (1991).
25. Frye, G. C., Ricco, A. J., Martin, S. J. & Brinker, C. J. in *Mater. Res. Soc.* (eds Brinker, C. J., Clark, D. E. & Ulrich, D. R.) 349–354 (Reno, Nevada, 1988).
26. Patel, G. N., Chance, R. R. & Witt, J. D. A planar-non-planar conformational transition in conjugated polymer solutions. *J. Chem. Phys.* **70**, 4387–4392 (1979).
27. Burns, A. R., Carpick, R. W., Sasaki, D. Y. & Shelhutt, J. A. Mechanochromism, shear force anisotropy, and molecular mechanics in polydiacetylene monolayers. *Tribol. Lett.* (in the press).
28. Fan, H. *et al.* Rapid prototyping of patterned functional nanostructures. *Nature* **405**, 56–60 (2000).
29. Brinker, C. J. Lu, Y., Sellinger, A. & Fan, H. Evaporation-induced self-assembly: nanostructures made easy. *Adv. Mater.* **11**, 579–585 (1999).
30. Day, D. R. & Lando, J. B. Conduction in polydiacetylene bilayers. *J. Appl. Polym. Sci.* **26**, 1605–1612 (1981).
31. Suzuoki, Y., Kimura, A. & Mizutani, T. in *Proc. 7th Int. Symp. Electrets* 850–855 (IEEE, New York, 1991).
32. Lu, Y. *et al.* Aerosol-assisted self-assembly of spherical, silica nanoparticles exhibiting hexagonal, cubic and vesicular mesophases. *Nature* **398**, 223–226 (1999).

Supplementary information is available from Nature’s World-Wide Website (<http://www.nature.com>) or as paper copy from the London editorial office of Nature.

**Acknowledgements**

We thank J. Curro and F. van Swol for technical discussions and T. Buechit for the nano-indentation results. This work was supported by the US Department of Energy Basic Energy Sciences Program, the Sandia National Laboratories Laboratory-Directed Research and Development Program, the National Aeronautics and Space Administration, the UNM/NSF Center for Micro-engineered Materials, and the Defense Advanced Research Projects Agency Bio-Weapons Defense Program. TEM investigations were performed in the Department of Earth and Planetary Sciences at the University of New Mexico. Sandia is a multiprogram laboratory operated by Sandia Corporation, a Lockheed-Martin Company, for the US DOE.

Correspondence and requests for materials should be addressed to C.J.B. (e-mail: [cjbrink@sandia.gov](mailto:cjbrink@sandia.gov)).

.....  
**Early Oligocene initiation of North Atlantic Deep Water formation**

**Richard Davies\*, Joseph Cartwright†, Jennifer Pike† & Charles Line\***

\* *ExxonMobil International Limited, St Catherine’s House, 2 Kingsway, PO Box 393, London WC2B 6WF, UK*

† *Department of Earth Sciences, PO Box 914, Cardiff University, Cardiff CF10 3YE, UK*

.....  
**Dating the onset of deep-water flow between the Arctic and North Atlantic oceans is critical for modelling climate change in the Northern Hemisphere<sup>1,2</sup> and for explaining changes in global ocean circulation throughout the Cenozoic era<sup>3</sup> (from about 65 million years ago to the present). In the early Cenozoic era, exchange between these two ocean basins was inhibited by the Greenland–Scotland ridge<sup>3,4</sup>, but a gateway through the Faeroe–Shetland basin has been hypothesized<sup>3,5</sup>. Previous estimates of the date marking the onset of deep-water circulation through this basin—on the basis of circumstantial evidence from neighbouring basins—have been contradictory<sup>5–9</sup>, ranging from about 35 to 15 million years ago. Here we describe the newly discovered Southeast Faeroes drift, which extends for 120 km parallel to the basin axis. The onset of deposition in this drift has been dated to the early Oligocene epoch (~35 million years ago) from a petroleum exploration borehole. We show that the drift was deposited under a southerly flow regime, and conclude that the**